

Solar filament eruptions and their physical role in triggering Coronal Mass Ejections

B. Schmieder, P. Démoulin, G. Aulanier

Observatoire de Paris, LESIA, 92195 Meudon France

Abstract

Solar filament eruptions play a crucial role in triggering coronal mass ejections (CMEs). More than 80% of eruptions lead to a CME. This correlation has been studied extensively during the past solar cycles and the last long solar minimum. The statistics made on events occurring during the rising phase of the new solar cycle 24 is in agreement with this finding. Both filaments and CMEs have been related to twisted magnetic fields. Therefore, nearly all the MHD CME models include a twisted flux tube, called a flux rope. Either the flux rope is present long before the eruption, or it is built up by reconnection of a sheared arcade from the beginning of the eruption.

In order to initiate eruptions, different mechanisms have been proposed: new emergence of flux, and/or dispersion of the external magnetic field, and/or reconnection of field lines below or above the flux rope. These mechanisms reduce the downward magnetic tension and favor the rise of the flux rope. Another mechanism is the kink instability when the configuration is twisted too much. In this paper we open a forum of discussions revisiting observational and theoretical papers to understand which mechanisms trigger the eruption. We conclude that all the above quoted mechanisms could bring the flux rope to an unstable state. However, the most efficient mechanism for CMEs is the loss-of-equilibrium or torus instability, when the flux rope has reached an unstable threshold determined by a decay index of the external magnetic field.

Keywords: active region, prominence, coronal mass ejection, MHD simulations of eruptions, electric currents

1. Introduction

It is widely accepted that solar prominences, with their overlying arcade system, are the progenitors of coronal mass ejections (CMEs) in the corona

Email address: brigitte.schmieder@obspm.fr (B. Schmieder, P. Démoulin, G. Aulanier)

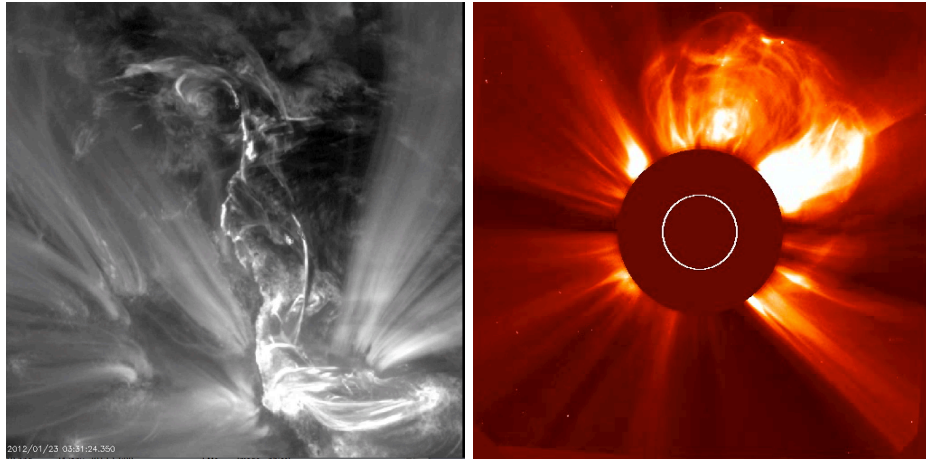


Figure 1: *Left panel:* Eruption of a filament observed on 23 January 2012 with the 171 Å SDO/AIA filter, just before a M9 class flare at 03:38 UT. *Right panel:* The associated CME observed with SOHO/LASCO C2. This event was very energetic with a large amount of accelerated protons (larger than 10 MeV) as registered by GOES. The 24 solar cycle was already very active at the beginning of 2012 with 7 active regions on the disk (Schmieder and Mein, 2012).

(Figure 1). Understanding their role in triggering CMEs is a major goal of solar physics. The relationship between filament eruption and other active solar phenomena such as flares or CMEs have been extensively investigated during the past years (*e.g.*, Subramanian and Dere, 2001; Chandra et al., 2010). Filaments/prominences are located either in active regions (ARs) or between ARs or in quiet Sun (like polar crown prominences). These three types of filaments are all frequently associated with CMEs. The rate of the association is very high according to the statistics made for different sets of events observed during the past solar cycles (56%, Jing et al., 2004; 83%, Gopalswamy et al., 2003; 92%, Hori and Culhane, 2002; 62%, Liu et al., 2012b).

The new solar cycle 24 started by the end of 2010, after a long solar minimum lasting nearly two years. Between the beginning of 2010 and the end of 2011, large long living ARs were observed (*e.g.*, Figure 2, Mandrini et al. 2012 in preparation). The long-lived ARs all had strong magnetic activity with flares, filament eruptions and CMEs (Schrijver et al., 2011; Liu et al., 2012c). Li et al. (2012) reported that 80 % of filament eruptions, occurring during the disk passage of a large AR in February 2010, were associated with CMEs. This is consistent with the statistics of the previous cycle.

Solar flares and CMEs are closely related to the coronal magnetic field. The plasma β (the ratio between thermal and magnetic pressure) is very small in the low solar corona, and the magnetic energy dominates all other forms of energies in the source regions of solar eruptions. The potential state (current free) magnetic field is the lower bound of energy for a given photospheric vertical field distribution. Since eruptions require magnetic energy release, the coronal

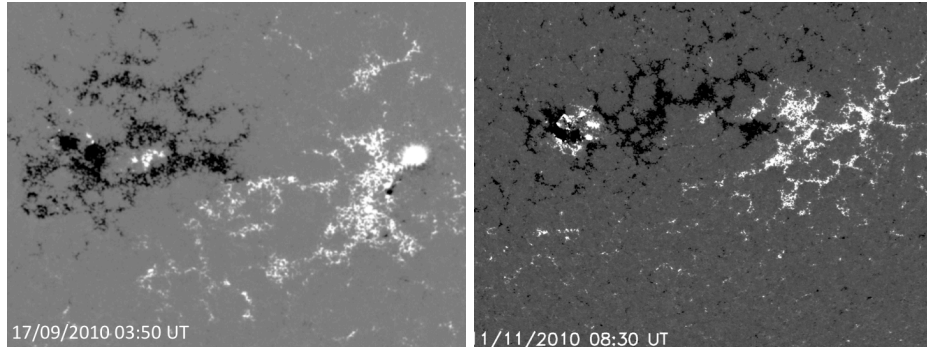


Figure 2: Emerging flux inserted in the negative following polarity of mature ARs during the rising phase of the solar cycle 24 observed with SDO/HMI magnetograph. *Left panel:* AR on 17 September 2010 at 03:50 UT. *Right panel:* AR on 11 November 2010 at 08:30 UT. White/black regions are positive/negative longitudinal magnetic field.

magnetic field must be highly non potential, *i.e.* with strong electric currents, prior to the eruption onset. There is much observational evidence in the solar atmosphere of the presence of such electric currents aligned along the magnetic field lines: either directly in the photosphere (*e.g.*, Liu et al., 2012a), or indirectly with the presence of J-shaped ribbons (*e.g.*, Chandra et al., 2009), X-ray sigmoids (Green et al., 2007; McKenzie and Canfield, 2008; Liu et al., 2010; Savcheva et al., 2012), twisted filaments/prominences (Williams et al., 2005; Koleva et al., 2012).

The MHD models of CMEs, commonly include a flux rope. In some of them, the flux rope is already set up in an equilibrium state long before the instability. The eruption occurs due to the evolution of the external magnetic field. The process could be: emerging flux (Chen, 1996; Chen et al., 2000; Jacobs et al., 2006; Manchester et al., 2008), reconnection of field lines below the flux rope (the tether-cutting model, Moore and Roumeliotis, 1992; Moore et al., 2001), or reconnection above the flux rope (the breakout model, Antiochos et al., 1999). Another possibility is the presence of an excessively twisted flux rope (kink instability, Török and Kliem, 2005; Kliem and Török, 2006). Then, many models start with the formation of a flux rope and bring it to an unstable state (Amari et al., 2000; Lin et al., 2001; Amari et al., 2005; Forbes et al., 2006; Fan and Gibson, 2007; Aulanier et al., 2010; Olmedo and Zhang, 2010; Zuccarello et al., 2012). There is also another type of CME model assuming a non-flux-rope magnetic structure prior to the eruption. In this type of models, the pre-eruption magnetic structure is a sheared core field instead of a flux rope (Antiochos et al., 1999). Nevertheless, the sheared core field is converted into a flux rope structure during the eruption through magnetic reconnection. As a result, magnetic flux ropes are an important structural component of CMEs.

Filament eruptions are well described by the classical 2D flux rope model CSHKP (Carmichael, 1964; Sturrock, 1966; Hirayama, 1974; Kopp and Pneuman, 1976) and visualized in limb observations (Cheng et al., 2011; Reeves and

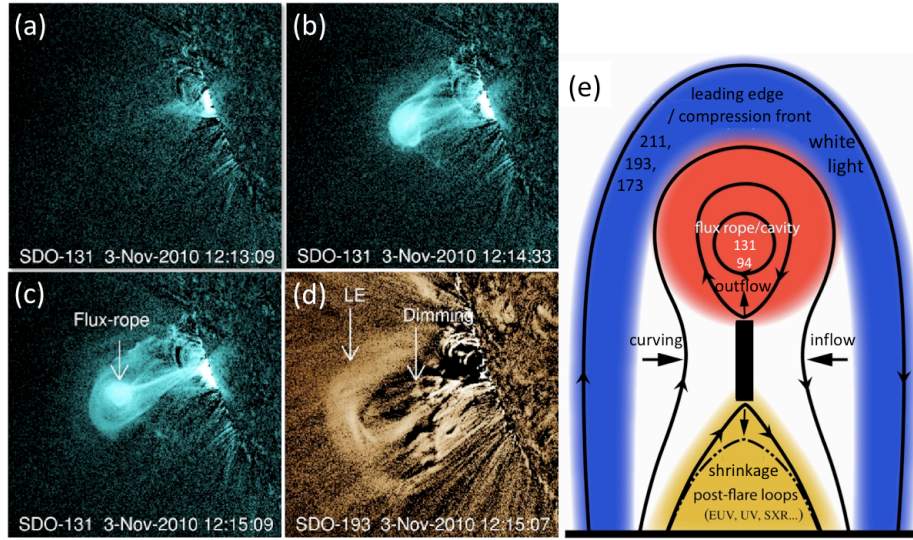


Figure 3: AIA 131 Å (~ 11 MK) base-difference images of the solar eruption on 3 November 2010 (light blue images) and an AIA 211 Å (~ 2 MK) image (brown image) showing the leading edge (LE) and the dimming. On the right, schematic drawing of the multi-temperature structures of the solar eruption as it is observed in the low corona by AIA (adapted from Cheng et al., 2011).

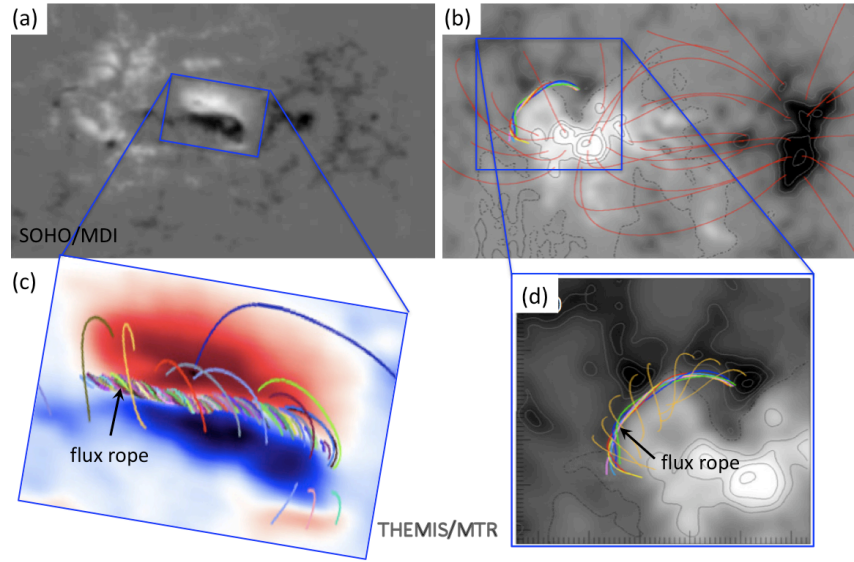


Figure 4: Non linear force-free magnetic extrapolation of vector magnetograms obtained by THEMIS/MTR showing the presence of a stable flux rope within two ARs. (a,b) Magnetograms of the vertical component. (c,d) Evidence of the flux rope in the extrapolation of the photospheric magnetograms (adapted from Canou et al., 2009; Guo et al., 2010a). (a) The emerging bipole in the center of an old AR has a "tongue" pattern, which is an indication of the emergence of a flux rope with positive magnetic helicity (Luoni et al., 2011).

Golub, 2011). An example is shown in Figure 3. The observations obtained with SDO/AIA filters show the formation and eruption of a flux-rope like structure. The flux rope is bright in AIA 131 Å images which represents emission of plasma at around 11 MK. In AIA 211 Å (2 MK) stretched loops are passing above the flux rope which is in the dark region (dimming). At this temperature the leading edge of the CME is bright due to the enhancement of plasma density by compression in front of the CME. In the sketch (Figure 3e), based on the classical model CSHKP, the different structures are represented schematically as they appear in the different filters of AIA: the ejection of the hot flux rope stretching upper field lines, the reconnection below the flux rope in a current sheet, and the formation of post-flare loops. These loops become cooler and cooler as they shrink (Forbes et al., 1989; Forbes and Acton, 1996; Aulanier et al., 2012).

The questions which arise from the above discussion are the following:

- Is a twisted flux tube (flux rope) present before the eruption?
- How a flux rope is formed above the photosphere?
- How is a flux rope brought to an eruptive state?

The present review is organized as following. We present in Section 2 a forum that discussed whether or not a flux rope exists prior to eruption. In Section 3, we review the eruption mechanisms. This summary is based on the possible triggering CMEs processes: emerging flux or shearing motions in the photosphere. Their coronal signatures in different temperatures or wavelengths is also considered. These arguments are based on observational as well as theoretical papers. In section 4, we focus on the eruption triggers. We conclude that the main trigger is the torus instability, which is also a loss of equilibrium. Moreover, it is argued that the kink instability alone cannot lead to a CME, while in some cases, it can bring the system to a loss of equilibrium. These two mechanisms are analyzed in details and we show some examples where the kink instability alone leads only to confined eruptions.

2. Presence of flux ropes

2.1. Evidence of flux ropes

Recent observations made with Hinode/SP (spectropolarimeter) based on the temporal rotation of magnetic vectors along an inversion line in an AR have been interpreted as the signature of a flux rope crossing the photosphere (Okamoto et al., 2008). During the emergence, velocity maps of granules obtained in Fe I 6302 Å have suggested that the flux rope was rising and the filament channel, represented by longitudinal magnetic field lower than 650 G, was enlarged during its passage through the photosphere (Okamoto et al., 2009). The interpretation of these observations is nevertheless uncertain and must be tested by simulations (see Section 2.3).

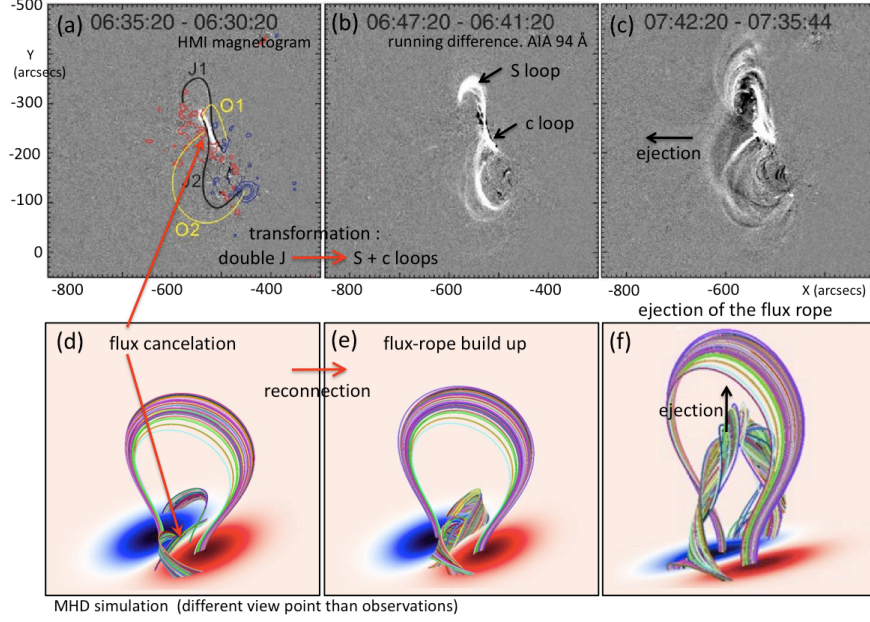


Figure 5: Build-up and eruption of a flux rope. (a-c) Formation and eruption of a sigmoid observed by AIA 94 Å near the Eastern solar limb. The presence of a sigmoid is the signature of strong currents aligned with the magnetic field (adapted from Liu et al., 2010). (d-f) MHD simulation showing the built up of a flux rope, by reconnection of field lines due to flux cancellation along the polarity inversion line and later on the flux rope eruption due to an ideal MHD instability (adapted from Amari et al., 2010). The observation and simulation panels have been selected to show a similar phase of the evolution.

Due to the non linearity of the force-free equation, it is difficult to find analytical solutions for non linear force-free field (NLFFF). Therefore, several numerical methods have been developed, such as the Grad-Rubin (Amari and Luciani, 1999; Wheatland, 2007; Canou et al., 2009; Amari et al., 2010), the upward integration (Wu and Guo, 1999), the magneto frictional (Valori et al., 2005; Kusano et al., 2012; Valori et al., 2012), the optimization (Wiegmann, 2008; Guo et al., 2010a, 2012), and the boundary element (Green’s function like, Yan, 1995) methods. Figure 4 shows two examples where flux rope have been evidenced using NLFFF extrapolations. van Ballegooijen (2004) proposed another method by inserting a flux rope in the magnetic region and led the system to relax using a magneto-frictional method. The application of the method to observed cases shows promising results (Savcheva and van Ballegooijen, 2009; Su et al., 2009; Savcheva et al., 2012; Su and van Ballegooijen, 2012). The MHD relaxation approach is used recently in global 3D extrapolation of the full disk magnetic field (Jiang et al., 2012).

Using the theoretical coronal flux rope models by Titov and Démoulin (1999) and Török and Kliem (2003), it has been shown that NLFFF extrapolation codes are capable of reconstructing significantly twisted flux ropes, as well as

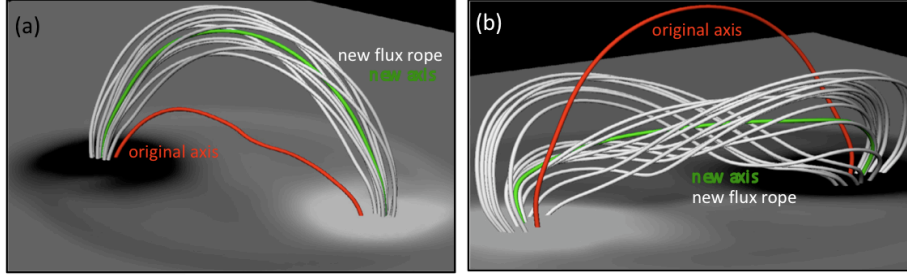


Figure 6: MHD simulation of the formation of a flux rope above the photosphere for two cases: (a) a weak strength of the magnetic field, (b) a higher strength of the magnetic field in the simulated flux rope located initially below the photosphere. In this simulation a flux rope below the photosphere is partly emerging and there is a restructuring/reconfiguration of the field above the photosphere in such a way that a new flux rope is created higher than the original flux rope axis in case (a) or below in case (b) (adapted from MacTaggart and Hood, 2010).

topological features of AR magnetic fields (Valori et al., 2005, 2010). Further more, NLFFF magnetic extrapolations are able to reconstruct a flux rope even in a complex magnetic topology from observed vector magnetograms (see Figure 4, Canou et al., 2009; Canou and Amari, 2010; Guo et al., 2010a).

2.2. Formation of active regions

Active regions are formed by flux emergence through the photosphere with the appearance, then separation of the polarities of many magnetic bipoles. Typically, they drift progressively apart and the polarities are collected in two main polarities revealing the global structure of the underlying flux tube (Zwaan, 1985; Strous et al., 1996; Pariat et al., 2004).

The two main polarities have typically some tongue shape during the emergence phase (López Fuentes et al., 2000; Chandra et al., 2009; Luoni et al., 2011, see Figure 4 top left). These elongated polarities are traces of the azimuthal component of the flux-rope field. By the end of the emergence phase, typically a few days for an AR with a flux around 10^{22} Mx, the tongues retract with the agglomeration of their magnetic flux in the corresponding magnetic polarity.

Magnetic dips are detected in the photosphere with vector magnetograms. They are loaded with dense material. The emergence can continue only when reconnection is occurring. It permits the downward escape of the dense plasma. The consequence of reconnection is detected as chromospheric brightenings and plasma flows (Pariat et al., 2004).

2.3. Some aspects of flux rope emergence above the photosphere

Local MHD simulations calculate the flux rope evolution from below the photosphere to the low corona (<10 Mm). The crossing of the photosphere by a flux rope is difficult for several reasons, first the flux rope is no longer buoyant, second, there is a change of regime from high to low β plasma, and finally, the

flux rope has a much larger radius than the local gravitational scale height, so that its weight becomes an important downward force which acts against emergence. The flux rope flattens below the photosphere and only fragmented sections can progressively reach the top of the photosphere (Manchester et al., 2004; Magara, 2006; Archontis et al., 2009).

The above difficulties for emergence were partly solved in the simulations of MacTaggart and Hood (2010, Figure 6). The rise of the flux rope leads progressively to small reconnections of field lines in the photosphere and finally to a magnetic reconfiguration, as follows. The emergence at and above the photosphere starts with sheared arcades. A pressure depression is present behind the flux rope. This drives converging flows toward the photospheric inversion line, and leads to reconnection of the arcade field lines. This implies the formation of a new flux rope above the photosphere. Depending on the parametric setting in the initial flux rope (within the convection zone), the new flux rope is formed above the previous one or below it (MacTaggart and Hood, 2010).

Finally, MHD simulations of an emerging flux rope show a pattern of magnetic tongues in the photosphere, similar to the observations of emerging ARs, especially the recent MHD simulations which start below the photosphere with a flux rope having a curved downward axis (Hood et al., 2009). As in observations, these tongues are present only during the emerging phase when the top part of the flux rope is only partly emerged above the photosphere (*e.g.*, Figure 6b).

3. Mechanisms bringing a flux rope into an unstable state

The precise origin of CMEs is still debated (*e.g.*, Schmieder and Aulanier, 2012). In the above section we have reviewed how a flux rope can be formed in the low corona. The presence of a flux tube indicated that the magnetic configuration has a large amount of free magnetic energy that can be released as a CME. What do we need to lift up the flux rope? The primary necessity is to decrease the magnetic tension which restrains the flux rope. There are two main processes to reduce the tension. First, by progressive reconnection below the flux rope. This is the tether cutting mechanism proposed by Moore and Roumeliotis (1992) and observed by Sterling and Moore (2004). Second, by removing the overlying arcades by coronal reconnection. This is the breakout model proposed by Antiochos et al. (1999) and observed by Aulanier et al. (1999).

Simulations of flux rope eruptions show the importance of the photospheric boundary conditions. Amari and Luciani (1999) modeled a configuration, which can support a prominence based on a flux rope embedded in an overlying, almost potential, arcade such that high electric currents are confined in the flux rope. This flux rope is formed by gradual photospheric diffusion of the magnetic field. When this process lasts for a long enough time, the magnetic configuration cannot stay in equilibrium and a CME ensues (Amari et al., 2000). Such photospheric diffusion of magnetic field prior to eruption was detected observationally by Schmieder et al. (2008). They observed the decrease of the

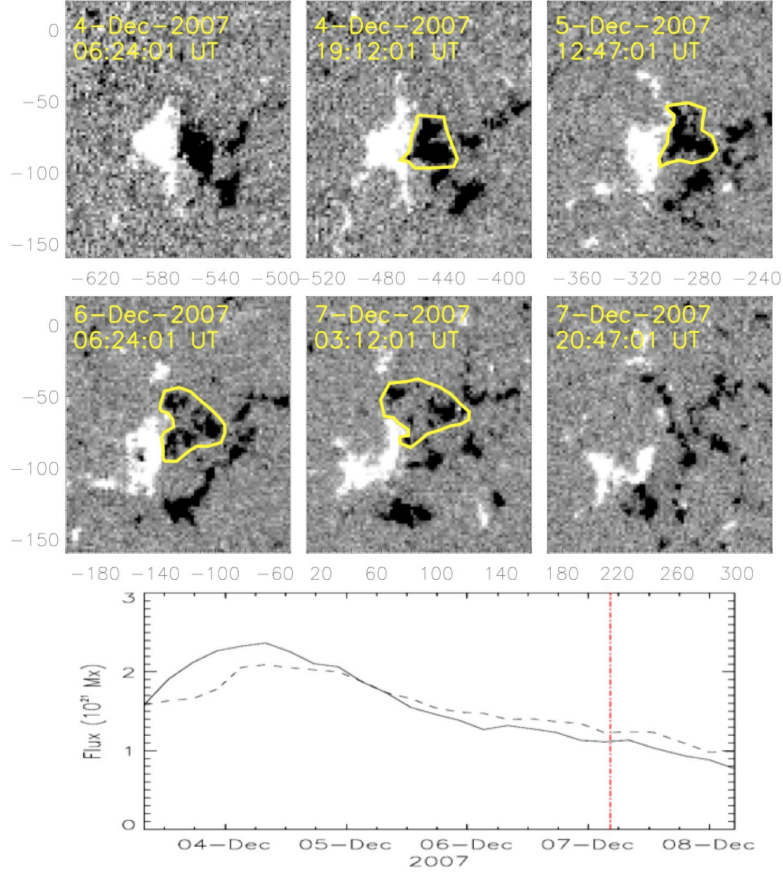


Figure 7: Dispersion of the magnetic field in an active region producing several CMEs. *Top panels:* MDI longitudinal derotated magnetograms of the AR during its disk passage. *Bottom panel:* Evolution of the magnetic flux of both AR polarities during four days. The red vertical line marks the onset of a CME during the decaying phase of the AR (adapted from Green et al., 2011).

magnetic field of the network, where the overlying arcades of the filament were anchored, during two days before the disappearance of a filament using THEMIS data. The decrease of the total strength in the field-of-view of THEMIS could be explained by the dispersion of the magnetic field during this time period. Green et al. (2011) measured the decrease of the flux in a decaying AR during the formation of a sigmoid leading to a CME (Figure 7). The long term diffusion of an AR was studied by Démoulin et al. (2002) and they reported that the rate of CMEs stayed nearly constant in the decaying AR during five months after the emergence phase.

In fact, in many studies, several mechanisms seem to work sequentially to bring the flux rope into an unstable state (Sterling et al., 2007, 2010, 2011). Wang and Shi (1993) have suggested a two-step magnetic reconnection process:

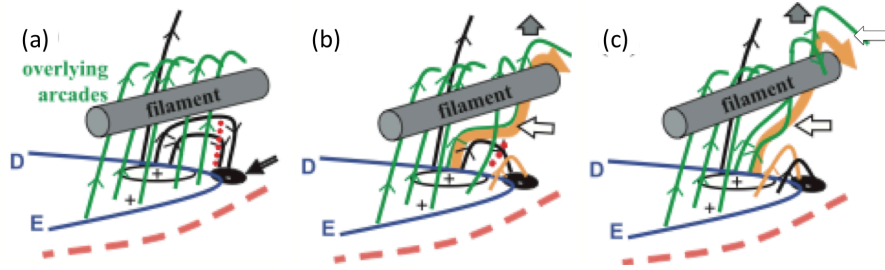


Figure 8: Schema of the three steps bringing a flux rope with overlying arcades in an unstable state at the edge of an AR. The dotted red line represents its photospheric inversion line. (a) Emerging magnetic flux represented by a bipole below the filament. (b) The emerging field lines reconnect with the arcade field line below the flux rope (indicated by the white arrows) implying a form of tether-cutting. (c) Above the flux rope, the overlying arcades reconnect with the nearby mature AR in a way similar to the breakout model. During the two last phases, the flux rope is rising as indicated by the grey arrows and small X ray flares are observed with Yohkoh (adapted from Nagashima et al., 2007).

the first step is a slow reconnection in the lower atmosphere that is observed as flux cancellation, while in the second step, the flare energy release comes from the fast reconnection higher in the corona. In the Nagashima et al. (2007) paper, the authors explained the observations of an X-ray flare and its associated CME by the presence of a large emerging flux in the decaying AR leading to a large erupting filament at the edge of the AR. The sketch presented in Figure 8 summarizes the different observed steps bringing the filament into an unstable state. Before the eruption there is an emerging flux that is reconnecting with an arcade overlying the filament. Small flares are also present before the eruption. Nagashima et al. (2007) pointed out the fact that these small flares occurred around the footpoints of the large filament but that no eruption was observed. They suggested that magnetic reconnection at the footpoints of the filament was not a sufficient condition for eruption. The small flares could be the signatures of tether cutting. Following up, a relatively small (C2.9) flare was interpreted as reconnection between the flux rope and the AR magnetic field, like in the break-out model. This last step brought the flux rope into an unstable phase leading finally to the CME and the X1.5 flare in this region. However, we note that the magnetic configuration needs to be close to the critical point for a loss-of-equilibrium to trigger the eruption.

During the solar minimum, many CMEs were initiated by eruptions of large polar crown filaments. Before eruption, a slow rise of filaments of the order of 1 km/s, during a few hours to one day, have been well observed with the high cadence instruments of STEREO and SDO/AIA (Gosain et al., 2009, 2012; Li et al., 2012). These observations can be directly explained by the loss-of-equilibrium model proposed by Forbes (1990) and Forbes and Isenberg (1991), where the flux rope progressively increases in height before erupting. We suggest that the slow and long-lasting ascending motion of the filament that is frequently observed corresponds to the change of the equilibrium height of the

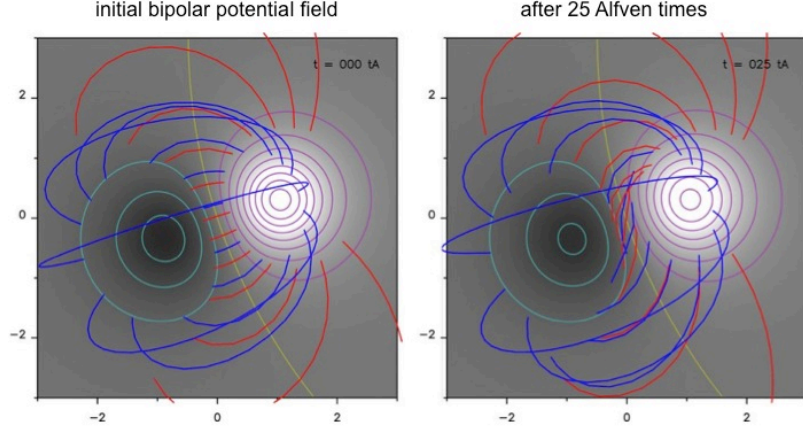


Figure 9: Initial conditions of the model of Aulanier et al. (2010) with a bipole consisting of two polarities with rotation motions at their periphery that creates a high magnetic shear along the photospheric inversion line (yellow line).

filament; then the filament approaches a critical point, as described in the loss-of-equilibrium model, and the eruption occurs.

4. Trigger mechanisms

As the magnetic configuration is not directly observed, only simulations, thus far, can test the different phenomena bringing the flux rope towards eruption. What is the respective role of emerging flux, twist, shear of the field lines and the reduced overlying magnetic field? Aulanier et al. (2010) used their simulation as a tool to distinguish the respective role of these different processes. The simulation starts with a bipole with rotating sunspots creating a high shear along the photospheric inversion line (Figure 9). Progressively a flux rope is formed by reconnection of low field lines like in the van Ballegoijen and Martens (1989) model. The reconnection at the photospheric inversion line is slowly driven by the applied photospheric diffusion of the magnetic field. As a consequence, the flux rope apex, quasi-statistically, increases its height until it reaches a critical point, and then it quickly erupts (Figure 10).

4.1. Analytic model of the torus instability

Let us understand, with an analytical analysis, the physical mechanisms which are working until the eruption in the Aulanier et al. (2010) simulation (Figure 11). The magnetic field of the global configuration can be decomposed in two components, as follows. The first component is the potential magnetic field created by the photospheric distribution of the vertical field component (magnetogram). The acting force of the potential field is a restraining force

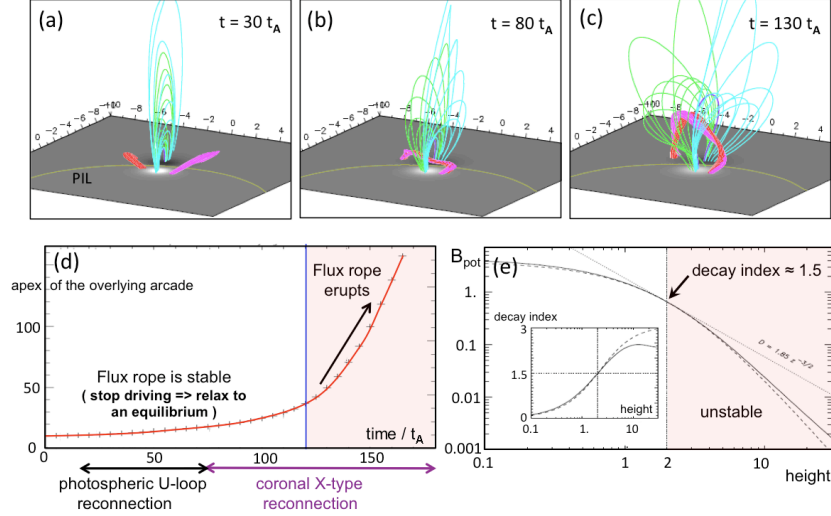


Figure 10: (a-c) MHD simulation of the formation and the eruption of a flux rope due to shearing motions and diffusion at the photospheric level. (a) Initial relaxed potential configuration (as in Figure 9a). (b) Formation of the flux rope (pink) after reconnection of the low field lines. (c) Beginning of the erupting phase. (d) Evolution of the arcade apex height versus time. (e) The potential field strength versus height and the decay index showing that for its value ~ 1.5 , the flux rope is unstable and can erupt (adapted from Aulanier et al., 2010).

directed downward. The second component of the field is the magnetic field created by the coronal net current and its subphotospheric image. This induces a magnetic force directed outward, known as the hoop force (it includes the repulsive force of the image current).

Aulanier et al. (2010) show that between $t=100$ and $120 t_A$ (Alfvén crossing time of the configuration), the system behavior is similar to the prediction of an electric circuit model (Figure 10). The flux rope approaches a critical point of the equilibrium curve driven by a constant increase of the twist (or by changing the magnetic flux below the flux rope). Their numerical model verifies the non equilibrium conditions analytically calculated with incomplete physics by van Tend and Kuperus (1978), Bateman (1978) and Kliem and Török (2006).

The critical point is estimated by the computation of a decay index, which represents the potential magnetic field drop-off along the vertical direction (z -axis):

$$n = -d \ln B / d \ln z$$

Török and Kliem (2007) found that the decay of the background magnetic field with height is a critical factor in determining whether the instability of the flux rope can result in an eruption or not, *i.e.*, the decay index must be larger than a critical value in order to have a successful eruption. The conditions are in accordance with the onset criteria expansion of the "torus instability" which can drive the free radial expansion of an electric current ring in axisymmetric

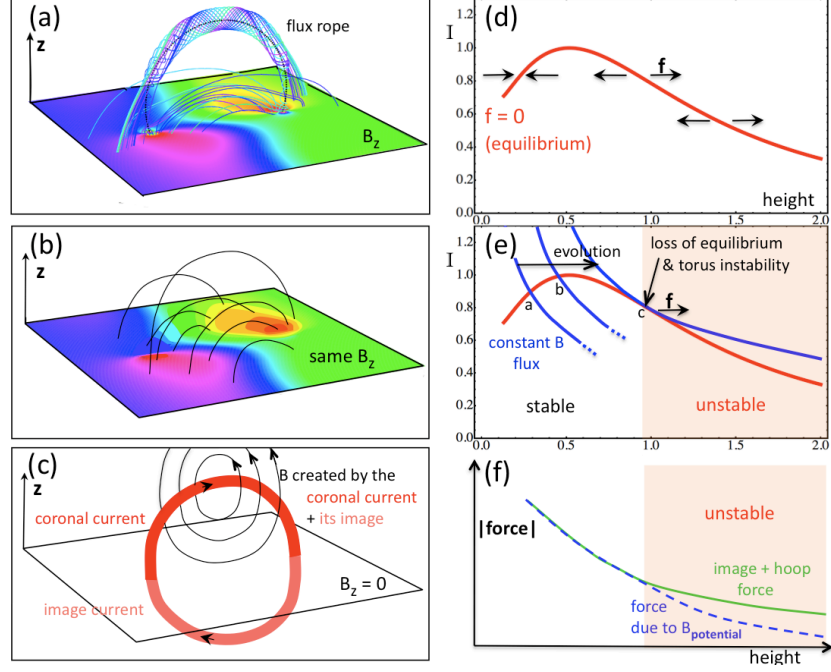


Figure 11: Analytical demonstration of the equivalence of a loss equilibrium and a torus instability. (a) Representation of the flux rope in equilibrium in a bipolar magnetic configuration. This magnetic field is decomposed in the sum of two magnetic field in (b) and (c). (b) Potential magnetic field associated to the normal field component B_z at the boundary. (c) Magnetic field created by only the coronal currents and their images (so that $B_z=0$ at the lower boundary). (d) Equilibrium curve (red line) with the current plotted versus height. The black arrows indicate the direction of the force in the vicinity of the equilibrium. (e) Evolution with the constraint of magnetic flux conservation until the loss of equilibrium (at point c), which is also the location of the torus instability. (f) The forces balance during the equilibrium, while the repulsion of the image current and the hoop force dominate in the unstable region leading to an upward ejection of the flux rope (adapted from Isenberg and Forbes, 2007; Démoulin and Aulanier, 2010).

circuit models (Figure 11). The instability occurs when the decrease in altitude of the downward magnetic tension becomes faster than of the upward magnetic pressure gradient.

4.2. Kink instability

The kink instability occurs when a flux rope is twisted above a threshold which depends on the twist profile and the aspect ratio of the flux rope. The kink instability typically leads to a flux rope eruption which saturates towards a certain height (Vršnak, 2008; Liu et al., 2012b) and could correspond to a failed eruption if no loss-of-equilibrium height was reached (Figure 12). Furthermore, numerical simulations demonstrate that the helical deformation enforces reconnection between legs of the flux rope if the initial twist is large enough (Kliem

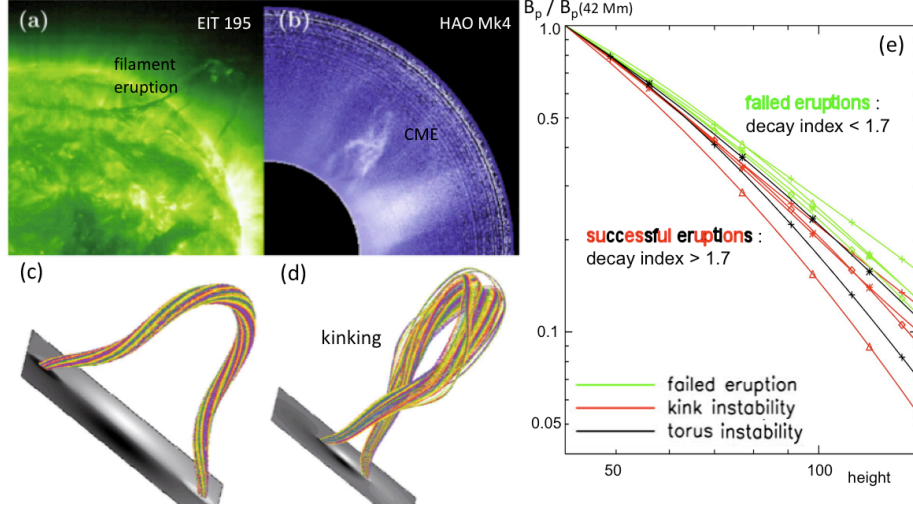


Figure 12: Kink and torus instability instabilities. (a) Eruption of a filament as seen in EUV. (b) The same filament, observed 22 minutes later by the coronagraph of HAO, as a kink shaped CME. (c,d) MHD simulation with an initial kink unstable flux rope with later the development of some inflation leading to a torus instability. (e) The potential field strength versus height for a set of observed eruptions. The decay index of successful eruptions is larger than 1.7, a value comparable with the model prediction (adapted from Török et al., 2010; Liu, 2008).

et al., 2010; Karlický and Kliem, 2010). Such a reconnection is complex since it involves also the magnetic field outside the flux rope.

Liu (2008) studied 10 events from different ARs, consisting of four failed eruptions, four eruptions due to kink instability, and two eruptions due to torus instability. They calculated the decay index of the background transverse magnetic field in the source AR and found that the decay index for successful eruptions is larger than the one for failed eruptions (Figure 12). Guo et al. (2010b) studied the decay index distribution with height of one confined eruption and found that the decay index is persistently smaller than 1.5 at a height ranging from 5 to 100 Mm above the photosphere. The magnetic configuration became kink unstable, and it started to rise at a height of 20 Mm. As a consequence of the low decay index, and thus the absence of the torus instability, the erupting filament did not evolve into a CME (Figure 13).

5. Conclusion

Many observations and simulations indicate that CMEs start with a flux rope eruption. Several mechanisms have been proposed involving flux emergence, or/and tether-cutting of field lines below the flux rope or/and photospheric diffusion of the magnetic field. However, we argue that all the above mechanisms are likely not sufficient to destabilize and eject the flux rope, so as

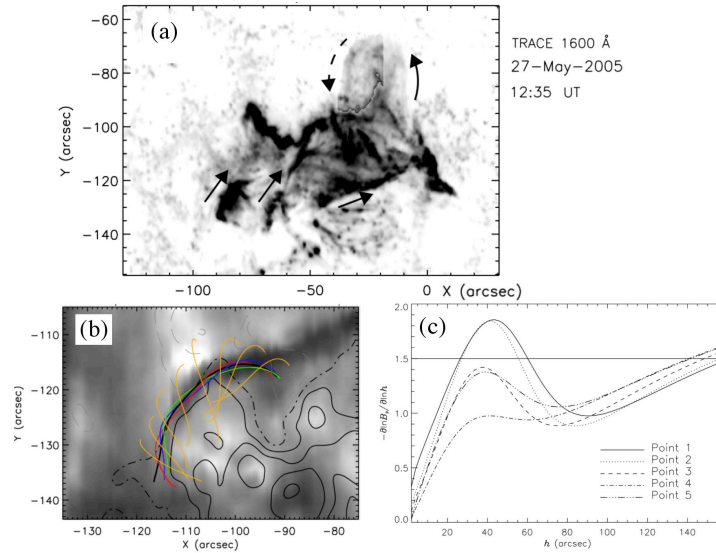


Figure 13: (a) Observation of a filament eruption using TRACE 1600 Å filter (reversed color table). The dark lanes are the bright ribbons, the faint lanes between the ribbons are the flare loops, the faint grey structure is the rising filament showing a kink shape. (b) Computed field lines, from a non-linear force-free extrapolation. They are drawn on top of an H_α image, showing a filament, and isocontours of the vertical component of the magnetic field (see Figure 4b,d). (c) The decay index versus height does not reach 1.5. It is the reason why the eruption felt (adapted from Guo et al., 2010a).

to trigger a CME. Several observations and numerical models indeed show that all these effects contribute in building a flux rope from sheared arcades. Then, slowly, the flux rope is lifted up in altitude. In addition, it is worth noticing that many examples show that the kink instability alone only leads to confined eruptions and cannot produce a CME. Actually, there is no simulation, to date, which produces a CME with the kink instability working alone. All previous mechanisms either bring the flux rope slowly (emergence, tether-cutting, diffusion), or rapidly (kink instability) to a loss of equilibrium, or equivalently a torus instability. This process leads in turn to the ejection of the flux rope and the creation of a CME.

References

- Amari, T., Aly, J.-J., Mikic, Z., Linker, J., 2010. Coronal mass ejection initiation: On the nature of the flux cancellation model. *Astrophys. J. Lett.* 717, L26–L30.
- Amari, T., Luciani, J. F., 1999. Confined Disruption of a Three-dimensional Twisted Magnetic Flux Tube. *Astrophys. J. Lett.* 515, L81–L84.
- Amari, T., Luciani, J. F., Aly, J. J., 2005. Non-Current-free Coronal Closure of Subphotospheric MHD Models. *Astrophys. J. Lett.* 629, L37–L40.

- Amari, T., Luciani, J. F., Mikic, Z., Linker, J., 2000. A Twisted Flux Rope Model for Coronal Mass Ejections and Two-Ribbon Flares. *Astrophys. J. Lett.* 529, L49–L52.
- Antiochos, S. K., DeVore, C. R., Klimchuk, J. A., 1999. A Model for Solar Coronal Mass Ejections. *Astrophys. J.* 510, 485–493.
- Archontis, V., Hood, A. W., Savcheva, A., Golub, L., Deluca, E., 2009. On the Structure and Evolution of Complexity in Sigmoids: A Flux Emergence Model. *Astrophys. J.* 691, 1276–1291.
- Aulanier, G., Démoulin, P., Mein, N., van Driel-Gesztelyi, L., Mein, P., Schmieder, B., 1999. 3-D magnetic configurations supporting prominences. III. Evolution of fine structures observed in a filament channel. *Astron. Astrophys.* 342, 867–880.
- Aulanier, G., Janvier, M., Schmieder, B., 2012. The standard flare model in three dimensions. I. Strong-to-weak shear transition in post-flare loops. *Astron. Astrophys.* 543, A110.
- Aulanier, G., Török, T., Démoulin, P., DeLuca, E. E., 2010. Formation of Torus-Unstable Flux Ropes and Electric Currents in Erupting Sigmoids. *Astrophys. J.* 708, 314–333.
- Bateman, G., 1978. MHD instabilities. The Massachusetts Institute of Technology.
- Canou, A., Amari, T., 2010. A Twisted Flux Rope as the Magnetic Structure of a Filament in Active Region 10953 Observed by Hinode. *Astrophys. J.* 715, 1566–1574.
- Canou, A., Amari, T., Bommier, V., Schmieder, B., Aulanier, G., Li, H., 2009. Evidence for a Pre-Eruptive Twisted Flux Rope Using the Themis Vector Magnetograph. *Astrophys. J. Lett.* 693, L27–L30.
- Carmichael, H., 1964. A Process for Flares. NASA Special Publication 50, 451.
- Chandra, R., Pariat, E., Schmieder, B., Mandrini, C. H., Uddin, W., 2010. How Can a Negative Magnetic Helicity Active Region Generate a Positive Helicity Magnetic Cloud? *Solar Phys.* 261, 127–148.
- Chandra, R., Schmieder, B., Aulanier, G., Malherbe, J. M., 2009. Evidence of Magnetic Helicity in Emerging Flux and Associated Flare. *Solar Phys.* 258, 53–67.
- Chen, J., 1996. Theory of prominence eruption and propagation: Interplanetary consequences. *J. Geophys. Res.* 101, 27499–27520.

- Chen, J., Santoro, R. A., Krall, J., Howard, R. A., Duffin, R., Moses, J. D., Brueckner, G. E., Darnell, J. A., Burkepile, J. T., 2000. Magnetic Geometry and Dynamics of the Fast Coronal Mass Ejection of 1997 September 9. *Astrophys. J.* 533, 481–500.
- Cheng, X., Zhang, J., Ding, M. D., Guo, Y., Su, J. T., 2011. A Comparative Study of Confined and Eruptive Flares in NOAA AR 10720. *Astrophys. J.* 732, 87.
- Démoulin, P., Aulanier, G., 2010. Criteria for Flux Rope Eruption: Non-equilibrium Versus Torus Instability. *Astrophys. J.* 718, 1388–1399.
- Démoulin, P., Mandrini, C. H., van Driel-Gesztelyi, L., Thompson, B. J., Plunkett, S., Kovári, Z., Aulanier, G., Young, A., 2002. What is the source of the magnetic helicity shed by CMEs? The long-term helicity budget of AR 7978. *Astron. Astrophys.* 382, 650–665.
- Fan, Y., Gibson, S. E., 2007. Onset of Coronal Mass Ejections Due to Loss of Confinement of Coronal Flux Ropes. *Astrophys. J.* 668, 1232–1245.
- Forbes, T. G., 1990. Numerical simulation of a catastrophe model for coronal mass ejections. *J. Geophys. Res.* 95, 11919–11931.
- Forbes, T. G., Acton, L. W., 1996. Reconnection and Field Line Shrinkage in Solar Flares. *Astrophys. J.* 459, 330.
- Forbes, T. G., Isenberg, P. A., 1991. A catastrophe mechanism for coronal mass ejections. *Astrophys. J.* 373, 294–307.
- Forbes, T. G., Linker, J. A., Chen, J., Cid, C., Kóta, J., Lee, M. A., Mann, G., Mikić, Z., Potgieter, M. S., Schmidt, J. M., Siscoe, G. L., Vainio, R., Antiochos, S. K., Riley, P., 2006. CME Theory and Models. *Space Science Reviews* 123, 251–302.
- Forbes, T. G., Malherbe, J. M., Priest, E. R., 1989. The formation flare loops by magnetic reconnection and chromospheric ablation. *Solar Phys.* 120, 285–307.
- Gopalswamy, N., Shimojo, M., Lu, W., Yashiro, S., Shibasaki, K., Howard, R. A., 2003. Prominence Eruptions and Coronal Mass Ejection: A Statistical Study Using Microwave Observations. *Astrophys. J.* 586, 562–578.
- Gosain, S., Schmieder, B., Venkatakrishnan, P., Chandra, R., Artzner, G., 2009. 3D Evolution of a Filament Disappearance Event Observed by STEREO. *Solar Phys.* 259, 13–30.
- Gosain, S. and Schmieder, B. and Artzner, G. and Bogachev, S. and Török, T., 2012, A Multi-spacecraft View of a Giant Filament Eruption during 2009 September 26/27, *Astrophys. J.* 761, 25.

- Green, L. M., Kliem, B., Török, T., van Driel-Gesztelyi, L., Attrill, G. D. R., 2007. Transient Coronal Sigmoids and Rotating Erupting Flux Ropes. *Solar Phys.* 246, 365–391.
- Green, L. M., Kliem, B., Wallace, A. J., 2011. Photospheric flux cancellation and associated flux rope formation and eruption. *Astron. Astrophys.* 526, A2.
- Guo, Y., Ding, M. D., Liu, Y., Sun, X.D. and DeRosa, M., Wiegmann, T., 2012. Modeling Magnetic Field Structure of a Solar Active Region Corona using Nonlinear Force-Free Fields in Spherical Geometry. *Astrophys. J.* 760, 47.
- Guo, Y., Ding, M. D., Schmieder, B., Li, H., Török, T., Wiegmann, T., Dec. 2010b. Driving Mechanism and Onset Condition of a Confined Eruption. *Astrophys. J. Lett.* 725, L38–L42.
- Guo, Y., Schmieder, B., Démoulin, P., Wiegmann, T., Aulanier, G., Török, T., Bommier, V., 2010a. Coexisting Flux Rope and Dipped Arcade Sections Along One Solar Filament. *Astrophys. J.* 714, 343–354.
- Hirayama, T., 1974. Theoretical Model of Flares and Prominences. I: Evaporating Flare Model. *Solar Phys.* 34, 323–338.
- Hood, A. W., Archontis, V., Galsgaard, K., Moreno-Insertis, F., 2009. The emergence of toroidal flux tubes from beneath the solar photosphere. *Astron. Astrophys.* 503, 999–1011.
- Hori, K., Culhane, J. L., 2002. Trajectories of microwave prominence eruptions. *Astron. Astrophys.* 382, 666–677.
- Isenberg, P. A., Forbes, T. G., 2007. A Three-dimensional Line-tied Magnetic Field Model for Solar Eruptions. *Astrophys. J.* 670, 1453–1466.
- Jacobs, C., Poedts, S., van der Holst, B., 2006. The effect of the solar wind on CME triggering by magnetic foot point shearing. *Astron. Astrophys.* 450, 793–803.
- Jiang, C., Feng, X., Xiang, C., 2012. A New Code for Nonlinear Force-free Field Extrapolation of the Global Corona. *Astrophys. J.* 755, 62.
- Jing, J., Yurchyshyn, V. B., Yang, G., Xu, Y., Wang, H., 2004. On the Relation between Filament Eruptions, Flares, and Coronal Mass Ejections. *Astrophys. J.* 614, 1054–1062.
- Karlický, M., Kliem, B., 2010. Reconnection of a Kinking Flux Rope Triggering the Ejection of a Microwave and Hard X-ray Source I. Observations and Interpretation. *Solar Phys.* 266, 71–89.
- Kliem, B., Linton, M. G., Török, T., Karlický, M., 2010. Reconnection of a Kinking Flux Rope Triggering the Ejection of a Microwave and Hard X-Ray Source II. Numerical Modeling. *Solar Phys.* 266, 91–107.

- Kliem, B., Török, T., 2006. Torus Instability. *Physical Review Letters* 96 (25), 255002.
- Koleva, K., Madjarska, M. S., Duchlev, P., Schrijver, C. J., Vial, J.-C., Buchlin, E., Dechev, M., 2012. Kinematics and helicity evolution of a loop-like eruptive prominence. *Astron. Astrophys.* 540, A127.
- Kopp, R. A., Pneuman, G. W., 1976. Magnetic reconnection in the corona and the loop prominence phenomenon. *Solar Phys.* 50, 85–98.
- Kusano, K. and Bamba, Y., Yamamoto, T., Iida, Y., Toriumi, S., 2012. Magnetic Field Structures Triggering Solar Flares and Coronal Mass Ejections. *Astrophys. J.* 760, 31.
- Li, L. P., Zhang, J., Li, T., Yang, S. H., Zhang, Y. Z., 2012. Study of the first productive active region in solar cycle 24. *Astron. Astrophys.* 539, A7.
- Lin, J., Forbes, T. G., Isenberg, P. A., 2001. Prominence eruptions and coronal mass ejections triggered by newly emerging flux. *J. Geophys. Res.* 106, 25053–25074.
- Liu, C., Deng, N., Liu, R., Lee, J., Wiegmann, T., Jing, J., Xu, Y., Wang, S., Wang, H., 2012a. Rapid Changes of Photospheric Magnetic Field after Tether-cutting Reconnection and Magnetic Implosion. *Astrophys. J. Lett.* 745, L4.
- Liu, K., Wang, Y., Shen, C., Wang, S., 2012b. Critical Height for the Destabilization of Solar Prominences: Statistical Results from STEREO Observations. *Astrophys. J.* 744, 168.
- Liu, R., Kliem, B., Török, T., Liu, C., Titov, V. S., Lionello, R., Linker, J. A., Wang, H., 2012c. Slow Rise and Partial Eruption of a Double-decker Filament. I. Observations and Interpretation. *Astrophys. J.* 756, 59.
- Liu, R., Liu, C., Wang, S., Deng, N., Wang, H., 2010. Sigmoid-to-flux-rope Transition Leading to a Loop-like Coronal Mass Ejection. *Astrophys. J. Lett.* 725, L84–L90.
- Liu, Y., 2008. Magnetic Field Overlying Solar Eruption Regions and Kink and Torus Instabilities. *Astrophys. J. Lett.* 679, L151–L154.
- López Fuentes, M. C., Démoulin, P., Mandrini, C. H., van Driel-Gesztelyi, L., 2000. The counterkink rotation of a non-Hale active region. *Astrophys. J.* 544, 540–549.
- Luoni, M. L., Démoulin, P., Mandrini, C. H., van Driel-Gesztelyi, L., 2011. Twisted Flux Tube Emergence Evidenced in Longitudinal Magnetograms: Magnetic Tongues. *Solar Phys.* 270, 45–74.
- MacTaggart, D., Hood, A. W., 2010. Simulating the "Sliding Doors" Effect Through Magnetic Flux Emergence. *Astrophys. J. Lett.* 716, L219–L222.

- Magara, T., 2006. Dynamic and Topological Features of Photospheric and Coronal Activities Produced by Flux Emergence in the Sun. *Astrophys. J.* 653, 1499–1509.
- Manchester, IV, W., Gombosi, T., DeZeeuw, D., Fan, Y., 2004. Eruption of a buoyantly emerging magnetic flux rope. *Astrophys. J.* 610, 588–596.
- Manchester, IV, W. B., Vourlidas, A., Tóth, G., Lugaz, N., Roussev, I. I., Sokolov, I. V., Gombosi, T. I., De Zeeuw, D. L., Opher, M., 2008. Three-dimensional MHD Simulation of the 2003 October 28 Coronal Mass Ejection: Comparison with LASCO Coronagraph Observations. *Astrophys. J.* 684, 1448–1460.
- McKenzie, D. E., Canfield, R. C., 2008. Hinode XRT observations of a long-lasting coronal sigmoid. *Astron. Astrophys.* 481, L65–L68.
- Moore, R. L., Roumeliotis, G., 1992. Triggering of Eruptive Flares - Destabilization of the Preflare Magnetic Field Configuration. In: Svestka, Z., Jackson, B. V., Machado, M. E. (Eds.), IAU Colloq. 133: Eruptive Solar Flares. Vol. 399 of Lecture Notes in Physics, Berlin Springer Verlag. p. 69.
- Moore, R. L., Sterling, A. C., Hudson, H. S., Lemen, J. R., 2001. Onset of the magnetic explosion in solar flares and coronal mass ejections. *Astrophys. J.* 552, 833–848.
- Nagashima, K., Isobe, H., Yokoyama, T., Ishii, T. T., Okamoto, T. J., Shibata, K., 2007. Triggering Mechanism for the Filament Eruption on 2005 September 13 in NOAA Active Region 10808. *Astrophys. J.* 668, 533–545.
- Okamoto, T. J., Tsuneta, S., Lites, B. W., Kubo, M., Yokoyama, T., Berger, T. E., Ichimoto, K., Katsukawa, Y., Nagata, S., Shibata, K., Shimizu, T., Shine, R. A., Suematsu, Y., Tarbell, T. D., Title, A. M., 2008. Emergence of a Helical Flux Rope under an Active Region Prominence. *Astrophys. J. Lett.* 673, L215–L218.
- Okamoto, T. J., Tsuneta, S., Lites, B. W., Kubo, M., Yokoyama, T., Berger, T. E., Ichimoto, K., Katsukawa, Y., Nagata, S., Shibata, K., Shimizu, T., Shine, R. A., Suematsu, Y., Tarbell, T. D., Title, A. M., 2009. Prominence Formation Associated with an Emerging Helical Flux Rope. *Astrophys. J.* 697, 913–922.
- Olmedo, O., Zhang, J., 2010. Partial Torus Instability. *Astrophys. J.* 718, 433–440.
- Pariat, E., Aulanier, G., Schmieder, B., Georgoulis, M. K., Rust, D. M., Bernasconi, P. N., 2004. Resistive emergence of undulatory flux tubes. *Astrophys. J.* 614, 1099–1112.
- Reeves, K. K., Golub, L., 2011. Atmospheric Imaging Assembly Observations of Hot Flare Plasma. *Astrophys. J. Lett.* 727, L52.

- Savcheva, A., Pariat, E., van Ballegoijen, A., Aulanier, G., DeLuca, E., 2012. Sigmoidal Active Region on the Sun: Comparison of a Magnetohydrodynamical Simulation and a Nonlinear Force-free Field Model. *Astrophys. J.* 750, 15.
- Savcheva, A., van Ballegoijen, A., 2009. Nonlinear Force-free Modeling of a Long-lasting Coronal Sigmoid. *Astrophys. J.* 703, 1766–1777.
- Schmieder, B., Aulanier, G., Jun. 2012. What are the physical mechanisms of eruptions and CMEs? *Adv. Spa. Res.* 49, 1598–1606.
- Schmieder, B., Bommier, V., Kitai, R., Matsumoto, T., Ishii, T. T., Hagino, M., Li, H., Golub, L., 2008. Magnetic Causes of the Eruption of a Quiescent Filament. *Solar Phys.* 247, 321–333.
- Schmieder, B., Mein, N., 2012. Le Soleil en fureur. *L’Astronomie* 48, 18–21.
- Schrijver, C. J., Aulanier, G., Title, A. M., Pariat, E., Delannée, C., Sep. 2011. The 2011 February 15 X2 Flare, Ribbons, Coronal Front, and Mass Ejection: Interpreting the Three-dimensional Views from the Solar Dynamics Observatory and STEREO Guided by Magnetohydrodynamic Flux-rope Modeling. *Astrophys. J.* 738, 167.
- Sterling, A. C., Chifor, C., Mason, H. E., Moore, R. L., Young, P. R., 2010. Evidence for magnetic flux cancelation leading to an ejective solar eruption observed by Hinode, TRACE, STEREO, and SoHO/MDI. *Astron. Astrophys.* 521, A49.
- Sterling, A. C., Moore, R. L., 2004. Evidence for Gradual External Reconnection before Explosive Eruption of a Solar Filament. *Astrophys. J.* 602, 1024–1036.
- Sterling, A. C., Moore, R. L., Berger, T. E., Bobra, M., Davis, J. M., Jibben, P., Kano, R., Lundquist, L. L., Myers, D., Narukage, N., Sakao, T., Shibasaki, K., Shine, R. A., Tarbell, T. D., Weber, M., 2007. Hinode Observations of the Onset Stage of a Solar Filament Eruption. *Pub. Astron. Soc. Japan* 59, 823–829.
- Sterling, A. C., Moore, R. L., Freeland, S. L., 2011. Insights into Filament Eruption Onset from Solar Dynamics Observatory Observations. *Astrophys. J. Lett.* 731, L3.
- Strous, L. H., Scharmer, G., Tarbell, T. D., Title, A. M., Zwaan, C., 1996. Phenomena in an emerging active region. I. Horizontal dynamics. *Astron. Astrophys.* 306, 947–959.
- Sturrock, P. A., 1966. Model of the High-Energy Phase of Solar Flares. *Nature* 211, 695–697.
- Su, Y., van Ballegoijen, A., 2012. Observations and Magnetic Field Modeling of a Solar Polar Crown Prominence. *Astrophys. J.* 757, 168.

- Su, Y., van Ballegooijen, A., Schmieder, B., Berlicki, A., Guo, Y., Golub, L., Huang, G., 2009. Flare Energy Build-up in a Decaying Active Region Near a Coronal Hole. *Astrophys. J.* 704, 341–353.
- Subramanian, P., Dere, K. P., Nov. 2001. Source Regions of Coronal Mass Ejections. *Astrophys. J.* 561, 372–395.
- Titov, V. S., Démoulin, P., 1999. Basic topology of twisted magnetic configurations in solar flares. *Astron. Astrophys.* 351, 707–720.
- Török, T., Berger, M. A., Kliem, B., 2010. The writhe of helical structures in the solar corona. *Astron. Astrophys.* 516, A49.
- Török, T., Kliem, B., 2003. The evolution of twisting coronal magnetic flux tubes. *Astron. Astrophys.* 406, 1043–1059.
- Török, T., Kliem, B., 2005. Confined and Ejective Eruptions of Kink-unstable Flux Ropes. *Astrophys. J. Lett.* 630, L97–L100.
- Török, T., Kliem, B., 2007. Numerical simulations of fast and slow coronal mass ejections. *Astronomische Nachrichten* 328, 743–746.
- Valori, G., Green, L. M., Démoulin, P., Vargas Domínguez, S., van Driel-Gesztelyi, L., Wallace, A., Baker, D., Fuhrmann, M., May 2012. Nonlinear Force-Free Extrapolation of Emerging Flux with a Global Twist and Serpentine Fine Structures. *Solar Phys.* 278, 73–97.
- Valori, G., Kliem, B., Keppens, R., 2005. Extrapolation of a nonlinear force-free field containing a highly twisted magnetic loop. *Astron. Astrophys.* 433, 335–347.
- Valori, G., Kliem, B., Török, T., Titov, V. S., 2010. Testing magnetofrictional extrapolation with the Titov-Démoulin model of solar active regions. *Astron. Astrophys.* 519, A44.
- van Ballegooijen, A. A., 2004. Observations and Modeling of a Filament on the Sun. *Astrophys. J.* 612, 519–529.
- van Ballegooijen, A. A., Martens, P. C. H., 1989. Formation and eruption of solar prominences. *Astrophys. J.* 343, 971–984.
- van Tend, W., Kuperus, M., 1978. The development of coronal electric current systems in active regions and their relation to filaments and flares. *Solar Phys.* 59, 115–127.
- Vršnak, B., 2008. Processes and mechanisms governing the initiation and propagation of CMEs. *Annales Geophysicae* 26, 3089–3101.
- Wang, J., Shi, Z., 1993. The flare-associated magnetic changes in an active region. II - Flux emergence and cancellation. *Solar Phys.* 143, 119–139.

- Wheatland, M. S., 2007. Calculating and Testing Nonlinear Force-Free Fields. *Solar Phys.* 245, 251–262.
- Wiegmann, T., 2008. Nonlinear force-free modeling of the solar coronal magnetic field. *J. Geophys. Res.* 113 (A12), 3.
- Williams, D. R., Török, T., Démoulin, P., van Driel-Gesztelyi, L., Kliem, B., 2005. Eruption of a Kink-unstable Filament in NOAA Active Region 10696. *Astrophys. J. Lett.* 628, L163–L166.
- Wu, S. T., Guo, W. P., 1999. Generation and propagation of solar disturbances: a magnetohydrodynamic simulation. *J. Atmos. Sol. Terr. Phys.* 61, 109–117.
- Yan, Y., Jun. 1995. The 3-D Boundary Element Formulation of Linear Force-Free Magnetic Fields with Finite Energy Content in Semi-Infinite Space. *Solar Phys.* 159, 97–113.
- Zuccarello, F., Meliani, Z., Poedts, S., 2012. Numerical Modeling of the initiation of coronal mass ejections in active region NOAA 9415. *Astrophys. J.* 758, 117–127.
- Zwaan, C., 1985. The emergence of magnetic flux. *Solar Phys.* 100, 397–414.